Electronic Supplementary Material (ESI) for Chemical Communications.

Electronic Supplementary Information

The Influence of the Enantiomeric Ratio of an Organic Ligand on the Structure and Chirality of Metal-Organic Frameworks

Iván Burneo,[a] Kyriakos C. Stylianou,[a] Inhar Imaz[a] and Daniel Maspoch[a,b*]

[a]*ICN2 – Institut Catala de Nanociencia i Nanotecnologia, Campus UAB, 08193 Bellaterra (Barcelona), Spain*

[b]*Institució Catalana de Recerca i Estudis Avançats (ICREA), 08100 Barcelona, Spain*

SI 1. Experimental section.

Materials. The following reagents were purchased from Sigma-Aldrich: 1,3,5-benzenetricarbonyl trichloride; L-aspartic acid dimethyl ester hydrochloride; triethylamine; lithium hydroxide monohydrate; and copper nitrate pentahydrate. D-aspartic acid dimethyl ester hydrochloride was purchased from Bachem S. and used as received. DMSO-*d* and chloroform-*d* for ^{1}H-NMR spectroscopy were purchased from Euriso-top® Cambridge Isotope Laboratories and used as received.

Synthesis of 1,3,5-benzene tricarbonyl tri-(*S*-(*L*-) or *R*-(*D*-)aspartic acid; *S*- *or R*-*BTAsp*).

Synthesis and characterisation of (1*S*,3*S*,5*S*)-1,3,5-benzenetricarbonyl tri-(***S*-(*L*-)**-aspartic dimethyl ester) *S-BTAsp-OMe* and (1*R*,3*R*,5*R*)-1,3,5-benzenetricarbonyl tri-(***R*-(*D*-)**-aspartic dimethyl ester) *R-BTAsp-OMe*.

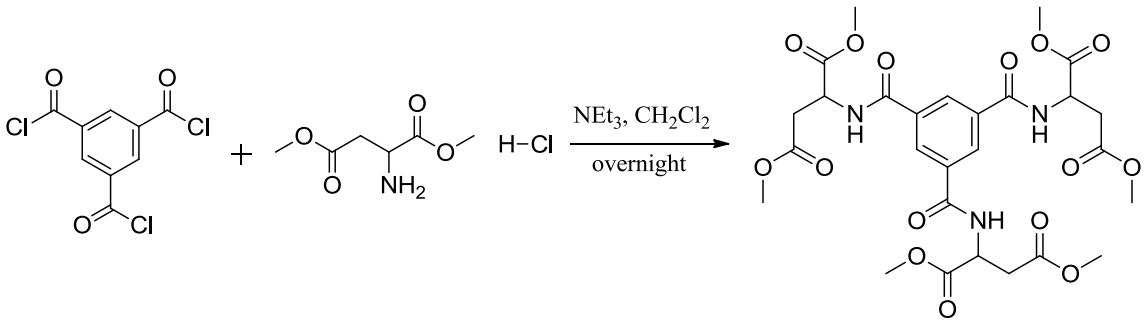

Both (1*S*,3*S*,5*S*)-1,3,5-benzenetricarbonyl tri-(*S*-(*L*-)aspartic dimethyl ester) and (1*R*,3*R*,5*R*)-1,3,5-benzenetricarbonyl tri-(*R*-(*D*-)aspartic dimethyl ester) were synthesised as previously reported.[1] *Preparation:* Dry triethylamine (4.24 mL, 30.13 mmol) was added to a cool solution (0 ^{o}C) of *S*-(*L*-) or *R*-(*D*-) aspartic acid dimethyl ester hydrochloride (2.71 g, 13.29 mmol) in dry CH_2Cl_2 (40 mL), and the resulting mixture was stirred for 20 min at 0 ºC. Then, a solution of 1,3,5-benzenetricarbonyl trichloride

(1.0 g, 3.69 mmol) in 30 mL of dry CH_2Cl_2 was added dropwise, and the reaction was stirred overnight. The reaction mixture was treated with CH_2Cl_2 (50 mL) and washed with aq. 2N H_2SO_4, followed by aq. $NaHCO_3$ and water. The organic layer was dried with anhydrous Na_2SO_4 and concentrated *in vacuo* to give 2.04 g of (1*S*,3*S*,5*S*)-1,3,5-benzenetricarbonyl tri-(*S*-(*L*-)aspartic dimethyl ester) (yield: 86%) or 2.01 g of (1*R*,3*R*,5*R*)-1,3,5-benzenetricarbonyl tri-(*R*-(*D*-)aspartic dimethyl ester) (yield: 85%). ^{1}H-NMR ($CDCl_3$, 250 MHz): 2.98-3.16(m, 6H), 3.71(s, 9H), 3.80 (s, 9H), 5.07-5.14(m, 3H), 7.65-7.68 (d, *J*=8.0 Hz, 3H), 8.22 (s, 3H). ^{13}C-NMR ($CDCl_3$, 62.9 MHz): 36.21, 49.80, 52.60, 53.42, 129.29, 134.87, 165.86, 171.75, 171.77. FT-IR (ATR, cm^{-1}): ṽ =3369.4, 3238.3, 2931.6, 2628.8, 2526.6, 1703, 1635.5, 1544.9, 1413.7, 1300, 1186, 921.9, 628.8, 574.7.

Saponification of (1*S*,3*S*,5*S*)-1,3,5-benzenetricarbonyl tri-(*S*-(*L*-)aspartic dimethyl ester) and (1*R*,3*R*,5*R*)-1,3,5-benzenetricarbonyl tri-(*R*-(*D*-)aspartic dimethyl ester) to give ***S*-BTAsp** or ***R*-BTAsp**.

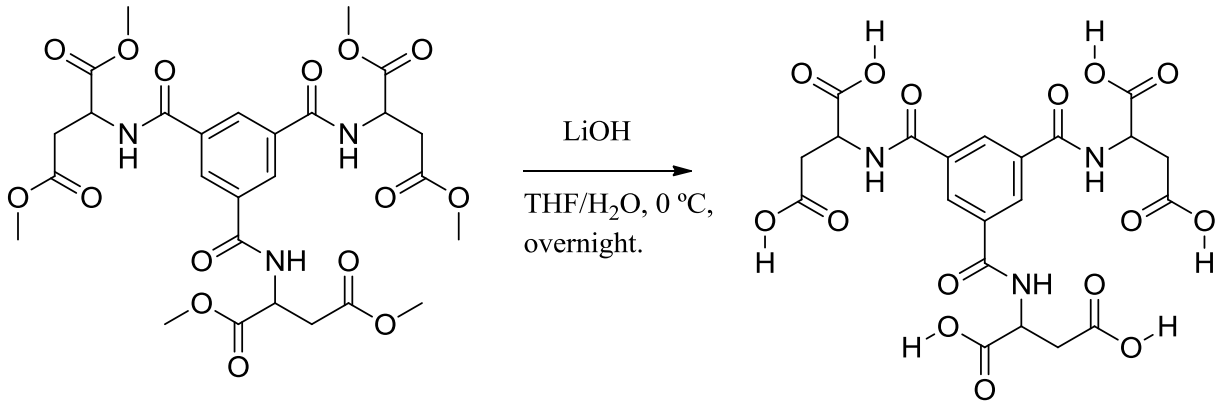

$LiOH{\cdot}H_2O$ (22.42 mmol) was added to a solution of (1*S*,3*S*,5*S*)-1,3,5-benzenetricarbonyl tri-(*S*-(*L*-)aspartic dimethyl ester) or (1*R*,3*R*,5*R*)-1,3,5-benzenetricarbonyl tri-(*R*-(*D*-)aspartic dimethyl ester) (3.20 mmol) in THF (20 mL) and H_2O (5 mL) at ~0 ^{o}C. The reaction mixture was stirred overnight at room temperature, and then acidified to pH ~3 with HCl (1.0 M). The mixture was washed with brine, dried over Na_2SO_4 and concentrated *in vacuo* to give 1.55 g (yield: 87%) of ***S*-BTAsp** or 1.56 g of ***R*-BTAsp** (yield: 87%).

^{1}H-NMR (D_2O, 250 MHz): 2.58-2.68 (m, 3H), 2.75-2.83 (m, 3H), 4.59-4.65(m, 3H), 8.34(s, 3H). ^{13}C-NMR (D_2O, 62.9 MHz): 39.91, 54.33, 129.69, 134.96, 168.74, 178.86, 179.41. FT-IR (ATR, cm^{-1}): $\tilde{\nu}$ = 3352, 1633.6, 1541, 1402.2, 1280.7, 1188. Elemental analysis for [$C_{21}H_{21}N_3O_{15}\cdot 4H_2O$] (***S*-BTAsp)** calculated (%): C: 40.20, H: 4.65, N: 6.70; found: C: 39.9, H: 4.7, N: 6.5 and [$C_{21}H_{21}N_3O_{15}\cdot 4H_2O$] (***R*-BTAsp)** calculated (%):C: 40.20, H: 4.65, N: 6.70; found: C: 38.6, H: 4.2, N: 6.1.

Synthesis of [Cu_3(*S*- or *R*-BTAsp)(H_2O)$_3$].12.75H_2O - ***S*** and ***R***.

To an aqueous solution (4 mL) of enantiopure *S*-BTAsp or *R*-BTAsp (10 mg, 0.02 mmol) was added $Cu(NO_3)_2\cdot 2.5H_2O$ (100 mg, 0.43 mmol). The mixture was brought to pH 6 using NaOH (1M) and became slightly cloudy. After 24 h at room temperature, greenish-blue octahedral crystals of ***S*** or ***R*** were obtained, and then filtered and air-dried to give 12.6 mg of ***S*** (yield: 67%, based on *S*-BTAsp) or 12.4 mg of ***R*** (yield: 70%, based on *R*-BTAsp). Elemental analysis for ***S*** - $[Cu_3(C_{21}H_{15}N_3O_{15})(H_2O)_3].(H_2O)_{12.75}$, calculated (%): C: 24.7, H: 4.6, N: 4.1; found: C: 26.3, H: 4.2, N: 4.1; and for ***R*** - $[Cu_3(C_{21}H_{15}N_3O_{15})(H_2O)_3].(H_2O)_{12.75}$, calculated (%): C: 24.7, H: 4.6, N: 4.1; found: C: 26.0, H: 4.0, N: 4.5.

Synthesis of [Cu_3(*RS*-BTAsp)(H_2O)$_4$].7.5H_2O - ***RS***.

To an aqueous solution (4 mL) of an equimolar mixture of *S*-BTAsp (5 mg, 0.01 mmol) and *R*-BTAsp (5 mg, 0.01 mmol) at pH 3.8 was added $Cu(NO_3)_2\cdot 2.5H_2O$ (100 mg, 0.43 mmol). The mixture was brought to pH 6 using NaOH (1M) and became slightly cloudy. After 15 to 17 days at room temperature, 5.8 mg of ***RS*** (yield: 35%, based on *S*-BTAsp) was obtained as greenish-blue, intergrown needle-type crystals. Elemental analysis for ***RS*** - $[Cu_3(C_{21}H_{15}N_3O_{15})(H_2O)_4].(H_2O)_{7.5}$, calculated (%): C: 26.6, H: 4.0, N: 4.4; found: C: 27.4, H: 4.6, N: 3.8.

SI 2. Characterisation.

Solution ^{1}H NMR spectra were obtained at the *Servei de Ressonància Magnètica Nucler at the Universitat Autònoma de Barcelona*. Routine ^{1}H and ^{13}C spectra were recorded on a Bruker AC250 (250 MHz for ^{1}H).

Elemental analyses were performed using a CHNS-O Elemental Analyzer 3011 (Eurovector). The ligands and MOFs were combusted at 1200 ºC in O_2 atmosphere, and the resulting samples were quantified by gas chromatography.

Single-crystal X-ray Diffraction (XRD) for ***S*** was collected on a Bruker AXS SMART Apex diffractometer with a CCD detector. The X–rays were generated using graphite monochromated Mo K*a* radiation from a molybdenum X–ray tube operating at 40 kV and 30 mA. The octahedral crystal was mounted on a fibre loop attached to the goniometer. Data were collected at 293 K. Single-crystal diffraction data for ***R*** and ***RS*** were collected at 150 K at beamline I19 at Diamond Light Source (DLS), at a wavelength of 0.6889 Å, using the Rigaku CrystalLogic Kappa goniometer at the zirconium absorption edge. Crystals were isolated in Fomblin-Y oil, and then mounted on MiTeGen loops. Both structures were resolved by direct methods and subsequently refined by correction of F^2 against all reflections, using SIR97, SHELXL97 and WinGX. Note: the H atoms of the guest H_2O molecules are omitted.

Table S1: Crystallographic data for ***S***, ***RS*** and ***R***.

Crystal data	***S***	***RS***	***R***
Empirical formula	$C_{21}H_{15}Cu_3N_3O_{30.75}$	$C_{42}H_{30}Cu_6N_6O_{53}$	$C_{21}H_{15}Cu_3N_3O_{30.75}$
Formula weight	991.99	1848.02	991.99
Temperature / K	293(2)	150	150
Crystal system	cubic	orthorhombic	cubic
Space group	F23	Pcnn	F23
a / Å	34.172(5)	17.530(3)	34.182(3)
b / Å	34.172(5)	20.037(3)	34.182(3)
c / Å	34.172(5)	21.050(3)	34.182(3)

α / °	90	90	90
β / °	90	90	90
γ / °	90	90	90
Volume / $Å^3$	39904(18)	7394(2)	39939(11)
Z	32	8	32
ρ_{calc} / mg mm^{-3}	1.321	1.660	1.320
μ / mm^-1	1.351	1.808	1.351
F(000)	4520.0	3374.0	4520.0
Crystal size / mm^3	0.61 × 0.32 × 0.32	0.56 × 0.34 × 0.22	0.38 × 0.2 × 0.2
Crystal colour and shape	Green-blue octahedra	Green-blue needles	Green-blue octahedra
Theta range for data collection	4.128 to 52.734°	4.95 to 52.74°	4.128 to 52.734°
Index ranges	$-42 \leq h \leq 42$, $-42 \leq k \leq 42$, $-42 \leq l \leq 42$	$-17 \leq h \leq 21$, $-24 \leq k \leq 23$, $-26 \leq l \leq 24$	$-42 \leq h \leq 18$, $-42 \leq k \leq 36$, $-39 \leq l \leq 37$
Reflections collected	140953	19582	30141
Independent reflections	6832	7428	6736
R(int) =	0.0711	0.0241	0.0485
Data/restraints/parameters	6832/0/360	7428/0/473	6736/0/360
Goodness-of-fit on F^2	1.323	1.048	1.196
Final R indices [$I > 2\sigma(I)$]	$R_1 = 0.0828$, $wR_2 = 0.2770$	$R_1 = 0.0659$, $wR_2 = 0.2013$	$R_1 = 0.0836$, $wR_2 = 0.2670$
Final R indices [all data]	$R_1 = 0.0920$, $wR_2 = 0.2926$	$R_1 = 0.0716$, $wR_2 = 0.2084$	$R_1 = 0.0897$, $wR_2 = 0.2775$
Largest diff. peak/hole (e $Å^{-3}$)	2.27/-0.72	1.68/-0.80	1.98/-0.73
Flack parameter	0.022(7)		0.073(8)

Powder X-ray Diffraction (PXRD) and *in-situ* Variable Temperature Powder X-ray Diffraction (VT-PXRD) patterns were recorded at room temperature on an X'Pert PRO MPD *θ/θ* powder diffractometer (PanAnalytical; configuration: convergent beam; radius: 240 mm) equipped with a

focalizing mirror and a transmission geometry with a spinner glass capillary sample holder, for Cu K_α radiation (λ = 1.5418 Å). For the VT-PXRD experiments, ***S*** and ***RS*** were packed and sealed inside a glass capillary tube (internal diameter: 0.3 mm).

Thermogravimetric Analysis (TGA): All analyses were performed in air, on an STA 449 F1 Jupiter– Simultaneous TGA-DSC from (NETZSCH; heating rate: 5 ºC/min; temperature range: 25 ºC to 500 ºC).

Field-Emission Scanning Electron Microscopy (FE-SEM): images were collected using a Quanta 650F Environmental Scanning Electron Microscopy (Field Emission Inc, USA). The samples were metallised with 10 nm of platinum in an EM ACE600 High-Vacuum Coater (Leica, Germany).

Electronic Circular Dichroism (ECD) spectra were measured using a J-715 CD spectrophotometer (JASCO) at room temperature (*ca.* 25 ºC). ECD experiments were performed in solution according to the following procedure: **a.** for ligands: 10 mg of *R*-BTAsp, *S*-BTAsp or an equimolar mixture of the two isomers were dissolved in 3.8 mL of water and HCl (200 µL, 0.5 M), and the resulting solutions were diluted in water to a final concentration of 0.05 mg/mL; **b.** for the MOFs: 10 mg of MOF (***R***, ***S*** or ***RS***) were first disassembled in 3.8 mL of water and HCl (200 µL, 0.5M), and the resulting solutions were diluted in water to a final concentration of 0.05 mg/mL. The spectra (obtained at 0.5 nm intervals) were smoothed using Savitsky-Golay algorithm with polynomial order 3 and a smoothing window of 30 points.

UV/Vis spectra for ***S***, ***R*** and ***RS*** were collected on a Cary 4000 UV/Vis spectrophotometer (Varian) equipped with a diffuse-reflectance accessory.

Fourier Transform Infra-Red (FT-IR) spectra were recorded on a Bruker Tensor 27FTIR spectrometer equipped with a Golden Gate diamond Attenuated Total Reflection (ATR) cell. The spectra were recorded in absorption mode at room temperature.

Vibrational Circular Dichroism (VCD) spectra were performed in a Bruker Tensor 27 FT-IR coupled to a PMA50 accessory, using an MIR long wavepass filter (1800 cm^{-1} to 600 cm^{-1}). Solid-phase samples were prepared using KBr pellets for IR and VCD (1 mg MOF in 100 mg KBr; 1% w/w). The crystalline material was mixed with dry KBr, finely ground, and then pressed at 10 tons for 5 min to make the pellet (diameter: 13 mm).

Gas sorption (CO_2/195 K, 273 K and 298 K; and N_2/77 K) measurements for ***S***, ***R*** and ***RS*** were performed using an AutosorbIQ. Samples were activated either by lyophilisation (-50 ^oC and 0.07 mbar) or by solvent exchange with $CHCl_3$ for 3 days, followed by outgassing at 40 ^oC under vacuum overnight.

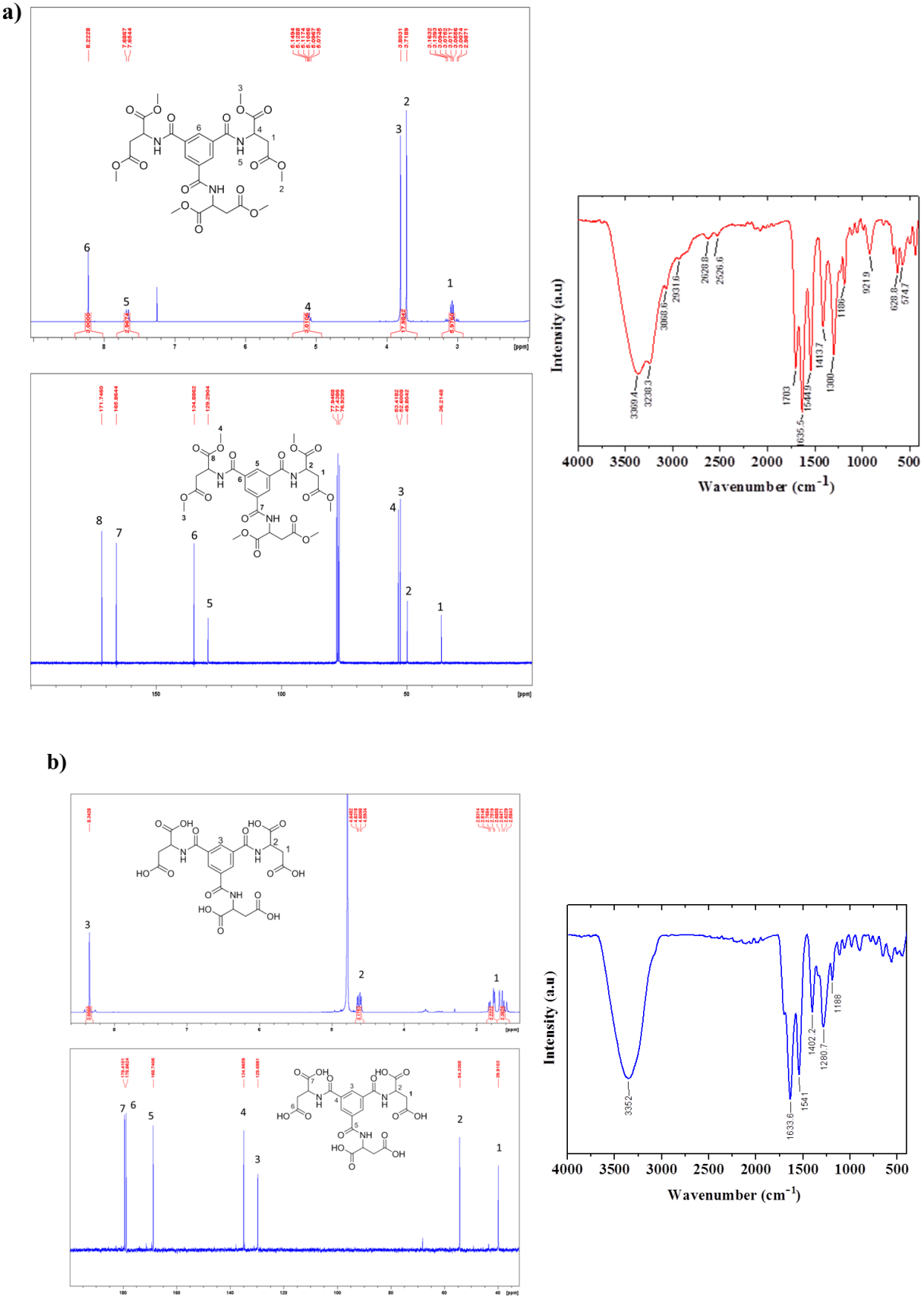

Figure S1: ^{1}H NMR spectra ($CDCl_3$) and corresponding FT-IR spectra of *S*-BTAsp-OMe (a) and *S*-BTAsp (b).

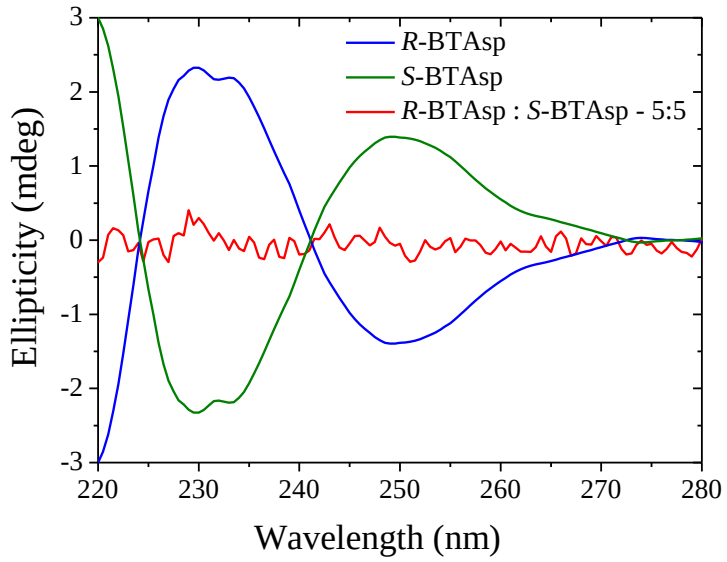

Figure S2: ECD spectra of aqueous solutions of free enantiopure *R*-BTAsp, free enantiopure *S*-BTAsp and an equimolar mixture of the two ligands.

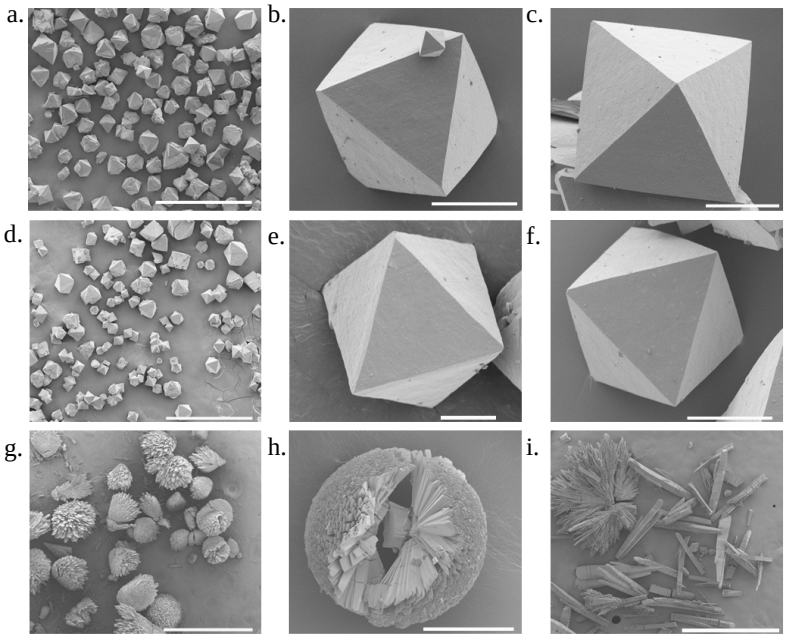

Figure S3: SEM images of (a-c) ***R***, (d-f) ***S*** and (g-i) ***RS***. The images reveal the octahedral morphology of the ***R*** and ***S*** crystals, and the intergrown, needle-shaped crystals of ***RS***, and confirm that all the MOFs are homogeneous. Scale bars: a) 400 μm; b) 30 μm; c) 20 μm; d) 400 μm; e) 10 μm; f) 30 μm; g) 1 mm; h) 50 μm; and i) 500 μm.

SI 3. The BTAsp ligand within *S*, *RS* and *R*.

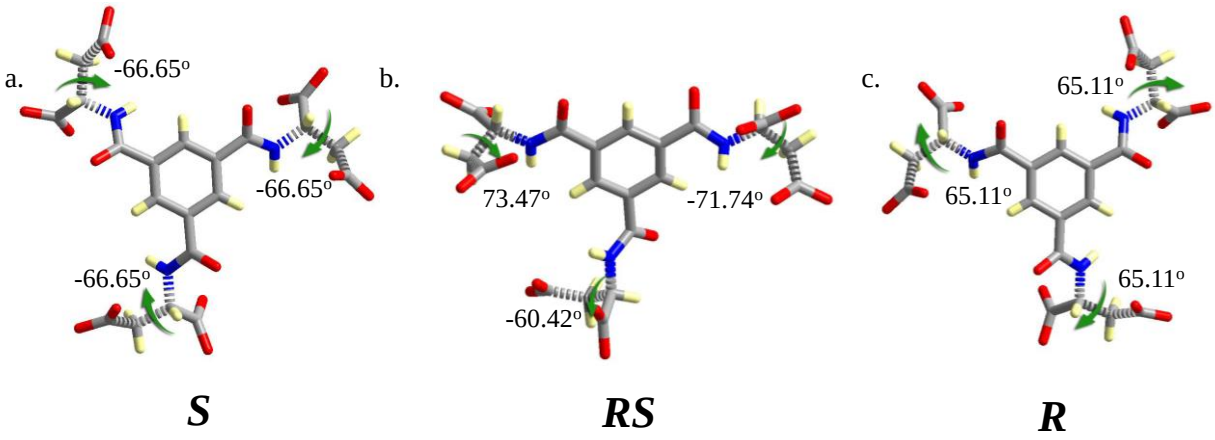

Figure S4: Representation of BTAsp within (a) ***S***, (b) ***RS*** and (c) ***R***. The dihedral side-chain angles of a single BTAsp ligand within ***S*** and ***R*** are equivalent (-66.65º and 65.11º, respectively), which confirms their opposite configuration and that the ligand is symmetric (*i.e.* the aspartate groups fold in the same manner). In contrast, the dihedral side-chain angles of the BTAsp ligand within ***RS*** are not equivalent: each aspartate residue folds in a different way, which highlights the flexibility of the ligand.

Table S2: Side-chain dihedral angles (χ_1) for ***S***, ***RS*** and ***R***.

Side-chain dihedral angle (χ_1)	***S***	***RS***	***R***
	−66.65º	73.47º	65.11º
	−66.65º	−71.74º	65.11º
	−66.65º	−60.42º	65.11º

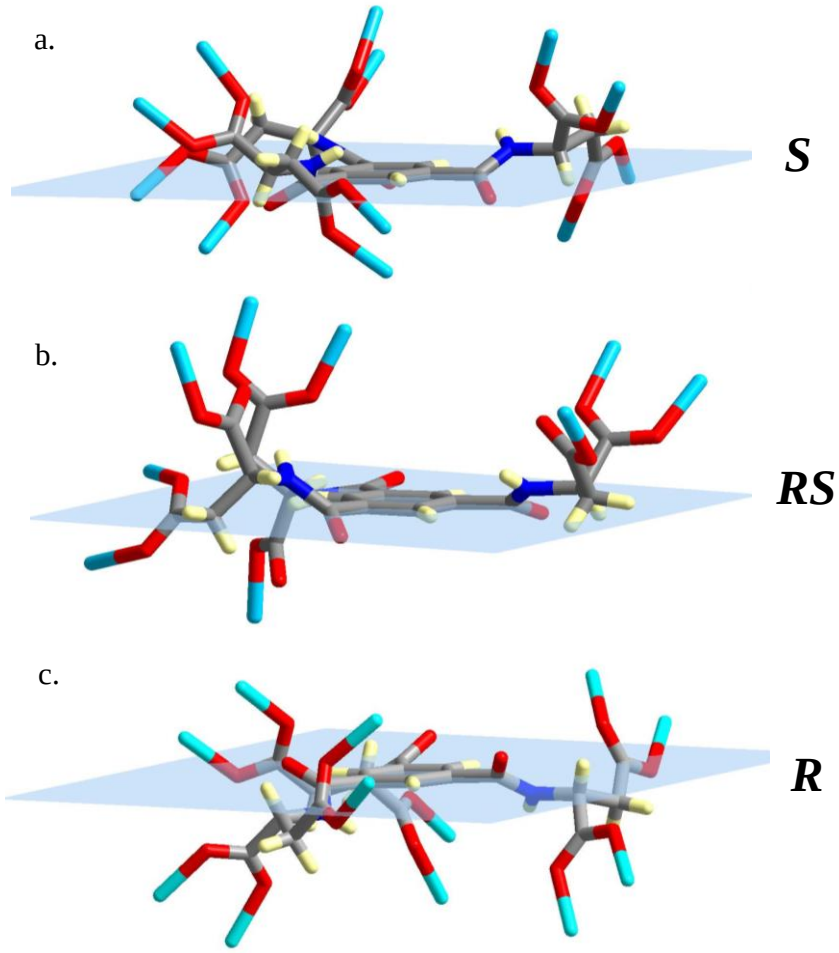

Figure S5: Illustration of the BTAsp ligand within (a) ***S***, (b) ***RS*** and (c) ***R***. The blue represents the plane (through the benzene ring) and confirms that the ligand is equivalent within ***S*** and ***R*** and symmetric, but within ***RS*** it is not so.

SI 4. Structure description of *S* and *R*.

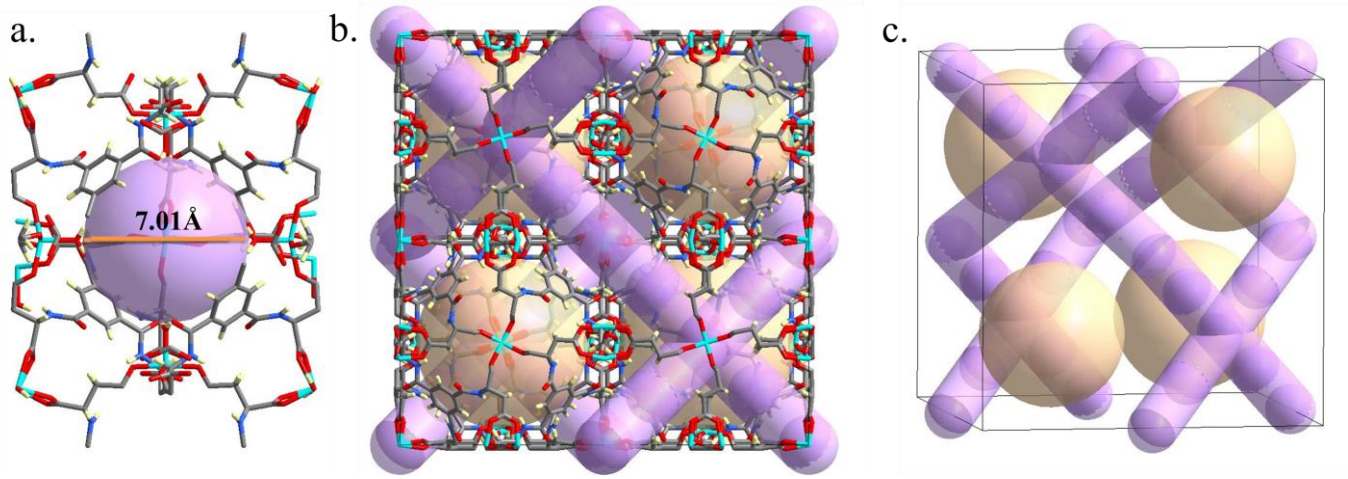

Figure S6: (a) Representation of the cavities formed in ***S*** (diameter: 7.01 Å). (b-c) 3D view of one unit cell, showing the organisation of the large isolated cages (yellow) and the cavities (purple); the latter are interconnected in 3D by pore openings (dimensions: 7.0 Å x 3.5 Å).

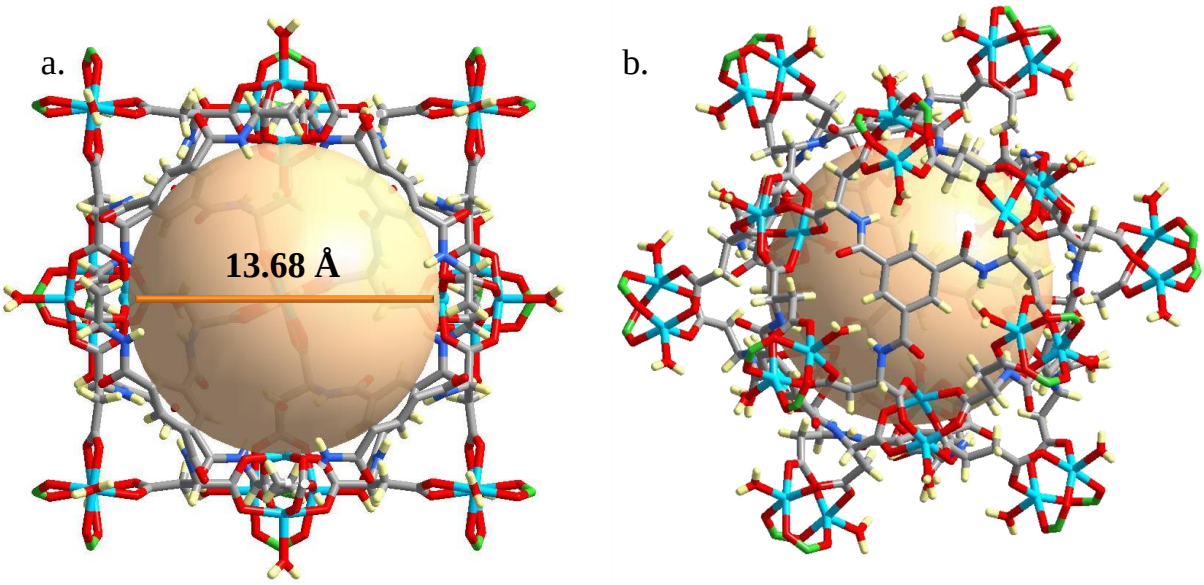

Figure S7: (a) Representation of one large isolated cage in ***S***. (b) Representation showing that each cage comprises eight BTAsp ligands and eighteen Cu-paddlewheels, twelve of which are shared with twelve neighbouring cages. The C atoms of the shared paddlewheels are coloured in green.

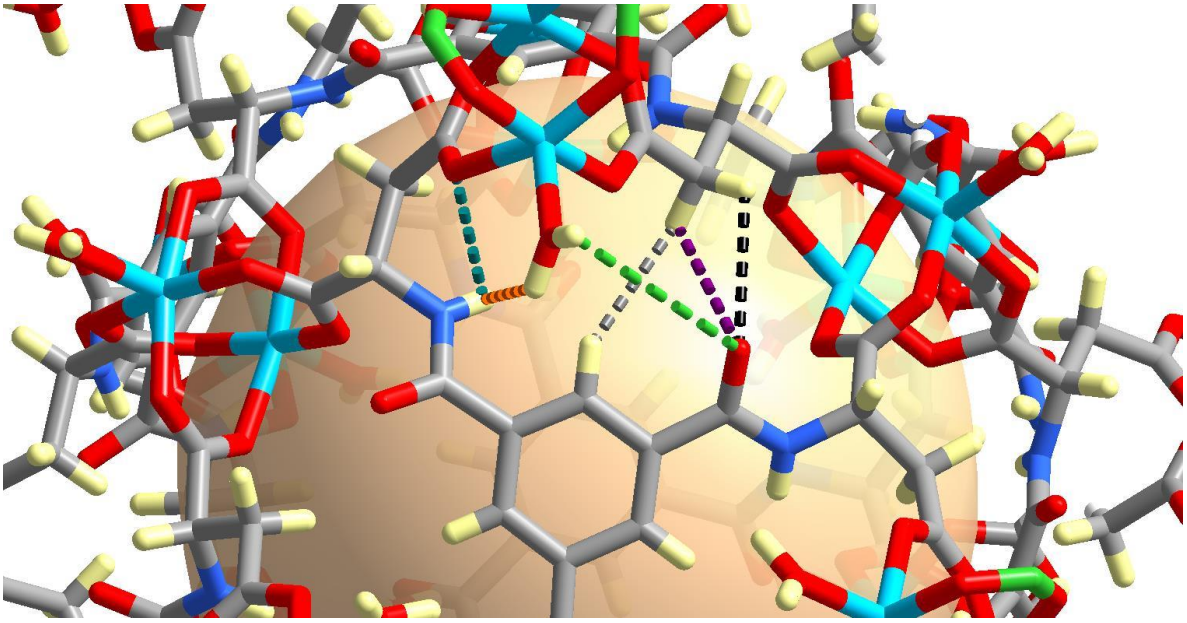

Atom-to-atom distance	**Colour**	**Bond distances (Å) (including van der Waals radii)**
NH···OC	blue	1.4
NH···HOH	orange	2.0
HOH···OC	green	3.4
CH···HCH	grey	0.5
HCH···OC	purple	0.3
HCH···OC	black	0.2

Figure S8: Representation of the bond distances within the isolated cages in ***S***, confirming the absence of any significant opening.

SI 5. Powder X-ray Diffraction.

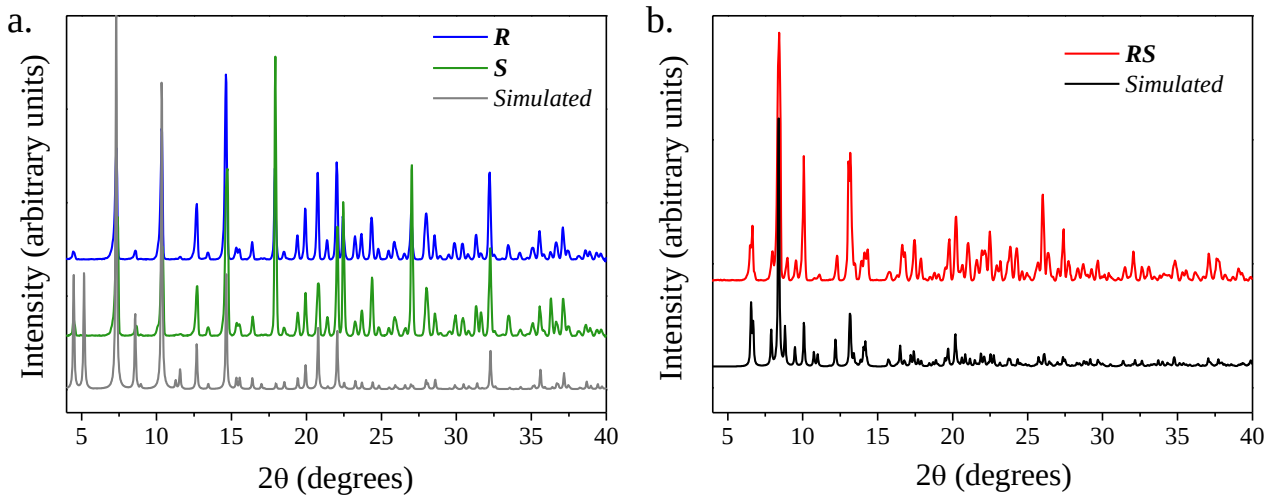

Figure S9: Comparison of the experimental PXRD patterns of (a) ***R*** and ***S***, and of (b) ***RS***, with their corresponding simulated PXRD pattern derived from the single-crystal XRD data. The excellent match indicates that all three MOFs were isolated as pure phases.

SI 6. ECD of *R*, *S* and *RS*.

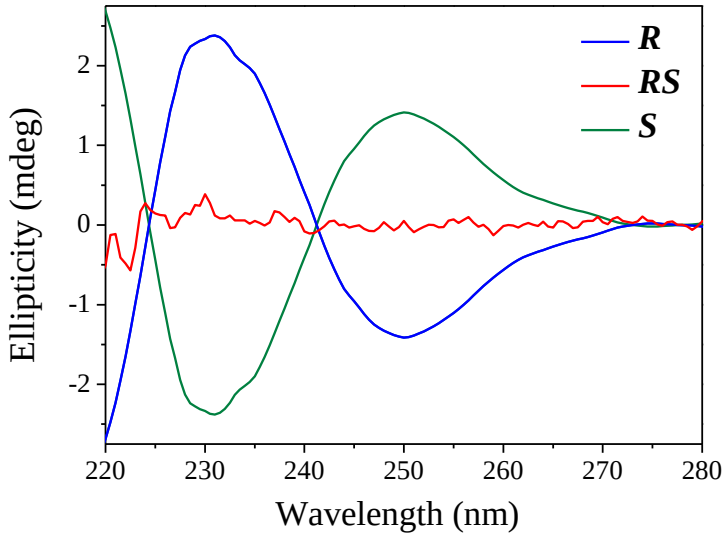

Figure S10: ECD spectra of the BTAsp ligand present within ***R***, ***S*** and ***RS*** after disassembly of each MOF at pH 2. The profiles are consistent with the corresponding ECD profiles of free *R*-BTAsp, free *S*-BTAsp and the equimolar mixture of the two ligands (see Figure S2).

SI 7. Structural characterisation of *RS*.

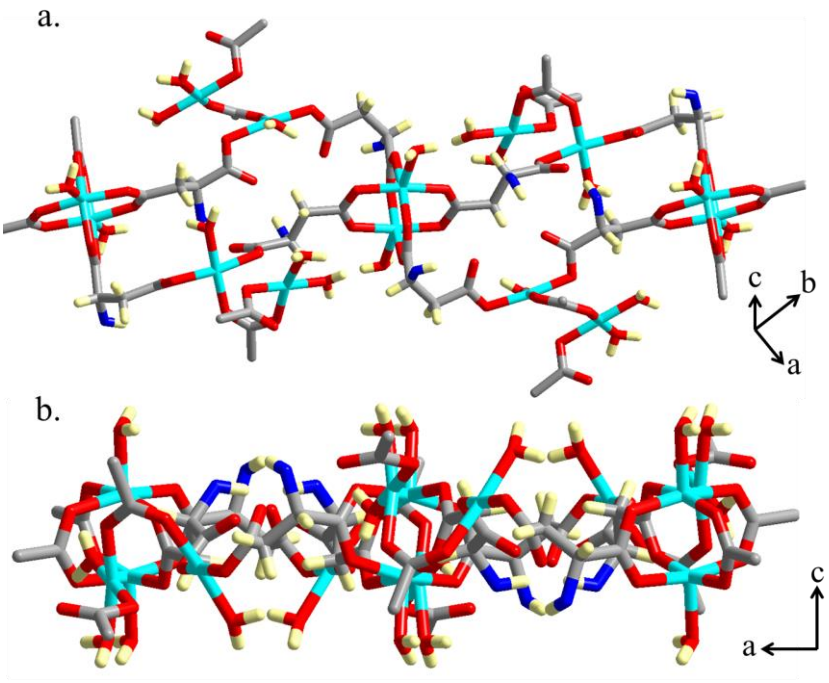

Figure S11: Illustration showing that the coordination of the aspartate groups within ***RS*** generates a 2D-Cu(II)-based layer running along the *b*-axis.

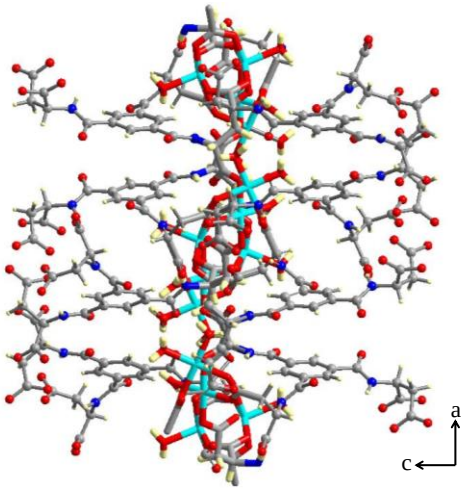

Figure S12: Illustration showing the organisation of the BTAsp ligand around the 2D-Cu(II)-based layer that produces the 3D ***RS***, in which the ligands are arranged in columns (as observed along the *b*-axis).

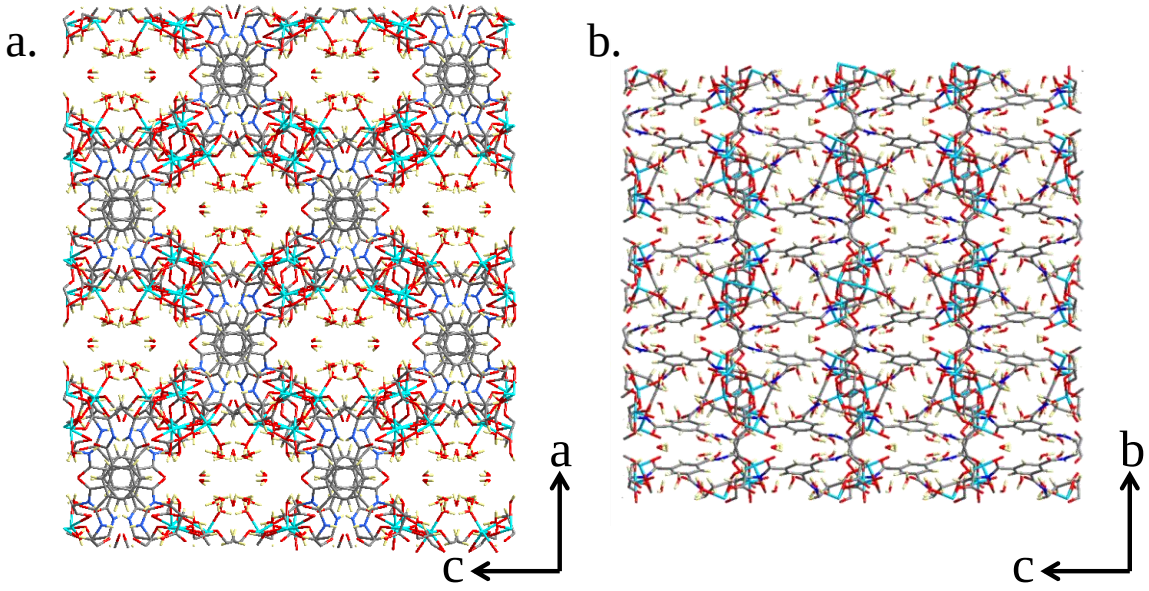

Figure S13: Packing of ***RS*** along the *b*-axis and the *a*-axis, showing that the 1D pores are filled with H_2O molecules and revealing the columnar arrangement of the BTAsp ligand (along the *b*-axis), respectively.

SI 8. ECD of *RS* made using *R*-BTAsp /*S*-BTAsp ratios of 7:3 or 6:4 (and *vice versa*).

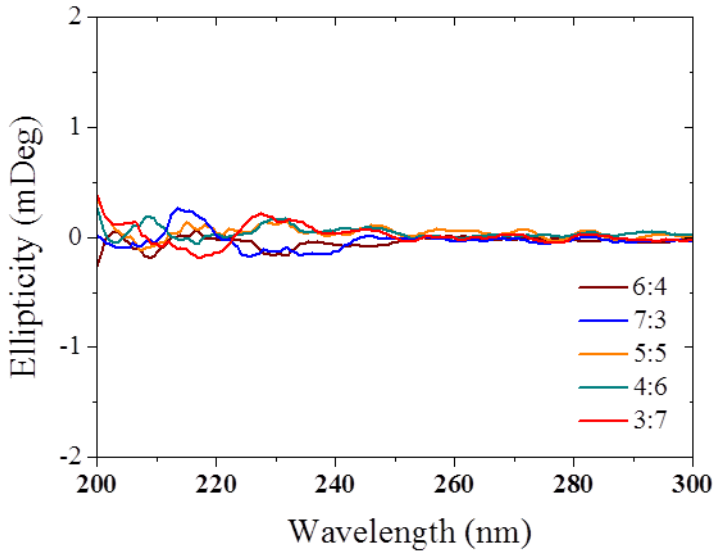

Figure S14: ECD spectra of the BTAsp ligand present in the ***RS*** crystals obtained when using *R*-BTAsp /*S*-BTAsp ratios of 7:3 or 6:4 (and *vice versa*), after their disassembly at pH 2. These profiles are consistent with the ECD profile of the equimolar mixture of *R*- and *S*-BTAsp and therefore, with the formation of ***RS*** (see Figure S10).

SI 9. Assessment of enantiomeric excess (*ee*).

The anisotropy factor (*g-factor*) is a concentration-independent parameter defined here as the ratio of ellipticity of the BTAsp ligand derived from circular dichroism, to its absorbance. It is also a function of the enantiomeric composition of the chiral ligand.[2,3] The g-factor is given by the following expression:

$$g = \frac{\Theta}{A} = \frac{\Delta\varepsilon \times c \times l}{\varepsilon \times c \times l} = \frac{\Delta\varepsilon}{\varepsilon}$$

where Θ is the ellipticity; Δε is the molar ellipticity; and ε is the molar extinction. The ellipticity values for each concentration and each ratio of *R*-BTAsp/*S*-*R*-BTAsp (free, or within the resulting MOFs) were collected by measuring the average of 60 points at λ = 231.5 nm.

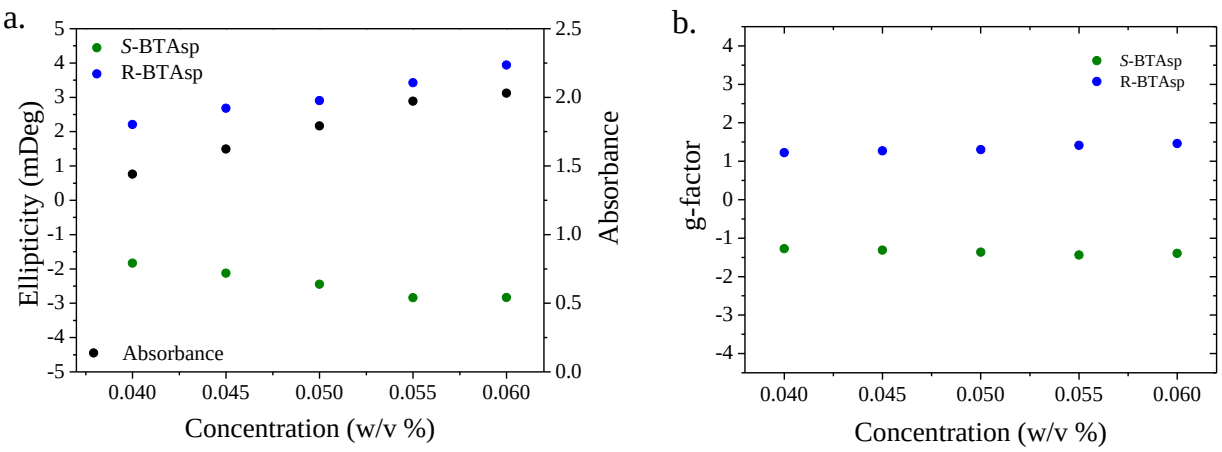

Figure S15: (a) Absorbance and ellipticity of enantiopure *R*-BTAsp or *S*-BTAsp ligand as a function of concentration. (b) The derived g-factor values plotted against the concentration of the pure ligand (*R*-BTAsp or *S*-BTAsp). Note that the g-factor values remain constant over the working concentration.

SI 10. Thermogravimetric Analysis (TGA) profiles of *R*, *S* and *RS*.

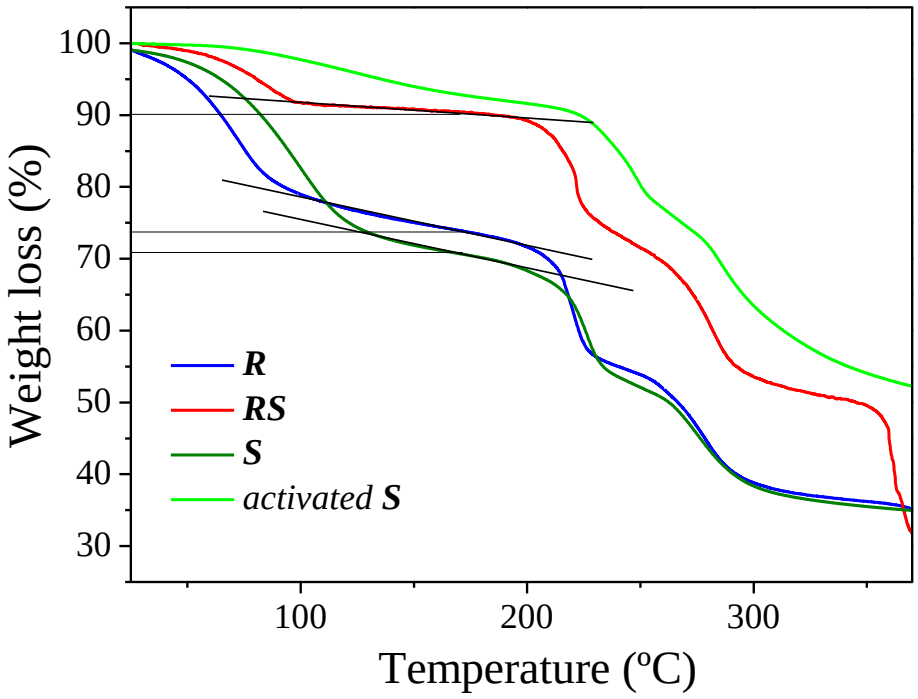

Figure S16: TGA curves for ***R***, ***S***, ***RS*** and activated ***S*** (heating rate: 5 ºC/min; temperature range: 25 to 400 ºC), showing that the profiles of ***R*** and ***S*** are very similar (continuous loss up to 200 ºC, corresponding to the loss of the guest H_2O molecules). Above this temperature, the framework collapses stepwise. In contrast, ***RS*** shows a weight loss of 9.8% from 30 ºC to 100 ºC, which corresponds to the loss of guest H_2O molecules; is stable up to 200 ºC; and then decomposes stepwise above 200 ºC. The TGA curve of the activated ***S*** shows no loss from 30 ºC to 100 ºC, which confirms that ***S*** is free of any guest molecules; this is followed by a weight loss of 7.1% that occurs before decomposition. The weight loss of 7.1 % may be due to the removal of H_2O molecules located either into the large cages and/or to the ones coordinated to Cu(II) centres within the amorphous solid.

SI 11. *In-situ* variable temperature PXRD of *S* and *RS*.

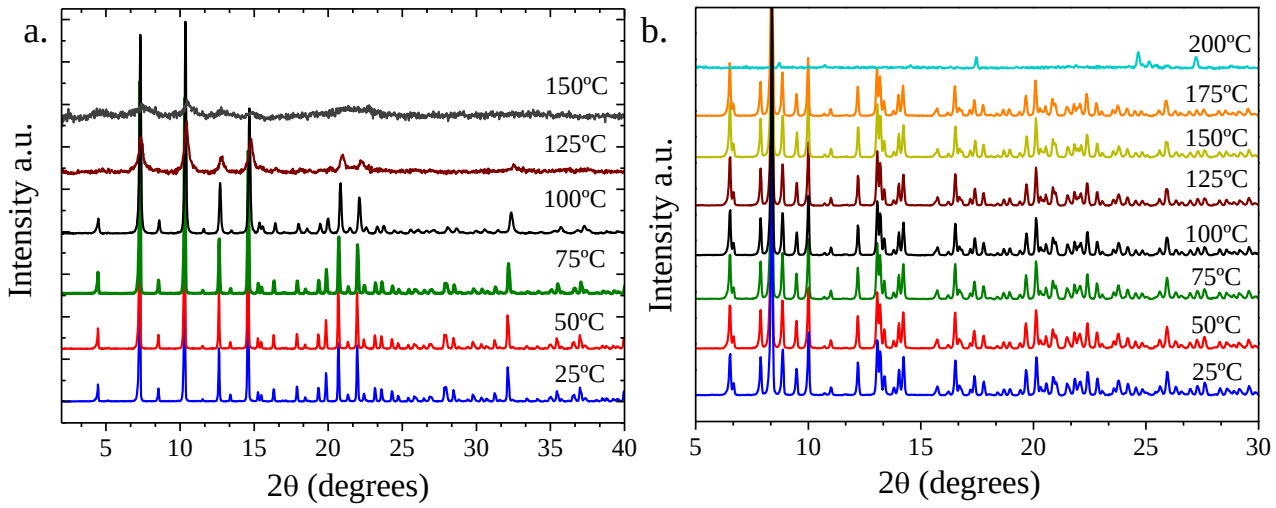

Figure S17: (a) *In-situ* variable temperature PXRD patterns of ***S*** sealed in a capillary tube, from 25 ºC to 150 ºC. As observed, ***S*** maintains its structural integrity up to 100 ºC. Above this temperature, ***S*** gradually collapses, which is consistent with the TGA data. (b) *In-situ* variable temperature PXRD patterns of ***RS*** sealed in a capillary tube, showing that it is thermally stable up to 175 ºC (*i.e.* at a much higher temperature than is ***S***). The loss of crystallinity observed from 175 ^{o}C to 200 ^{o}C reveals that ***RS*** collapses rapidly, presumably due to the loss of the coordinated H_2O molecules to Cu(II). This observation is in excellent agreement with the TGA profile of ***RS***.

SI 12. Stability of *RS* and *S*.

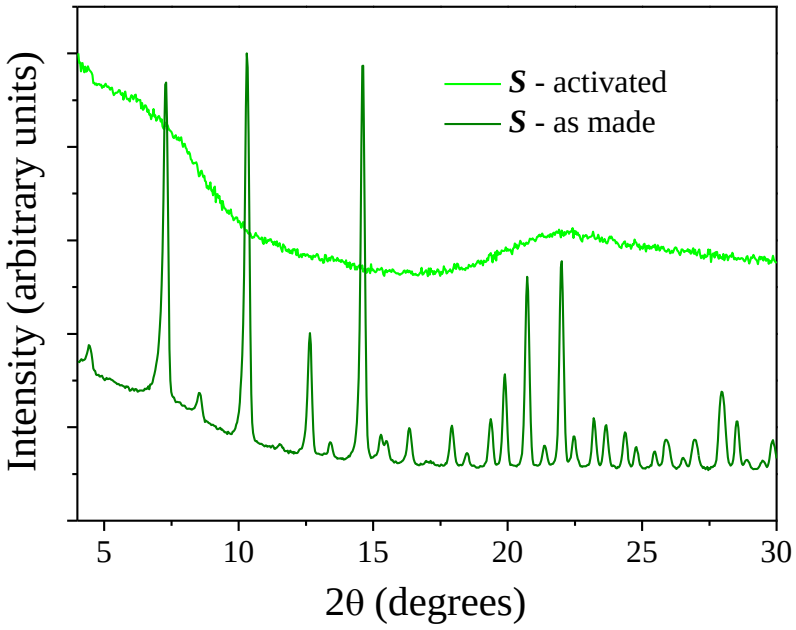

Figure S18: PXRD spectra revealing that upon activation-lyophilisation, ***S*** becomes irreversibly amorphous.

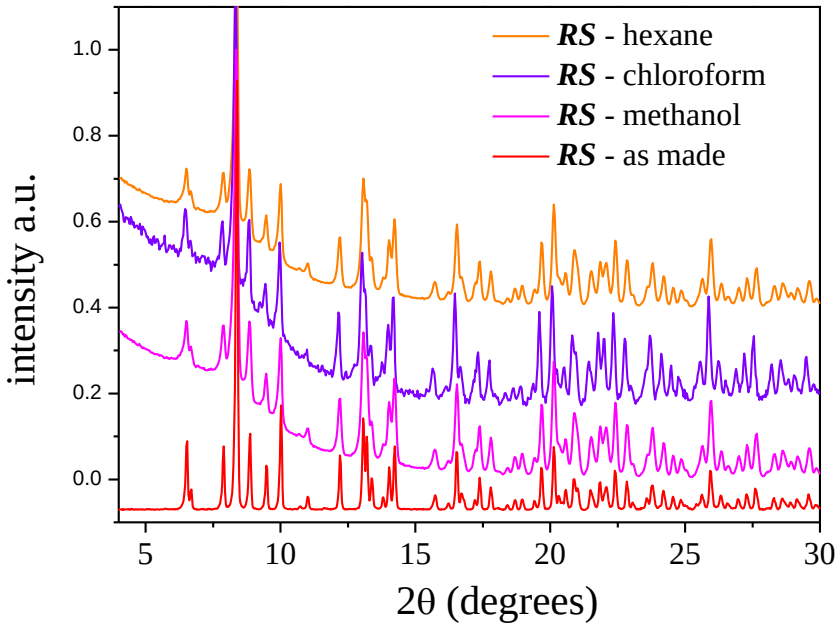

Figure S19: PXRD spectra showing that ***RS*** is stable after its immersion in various organic solvents (methanol, chloroform or hexane) for at least 3 days.

SI 13. Sorption study of S, RS and R

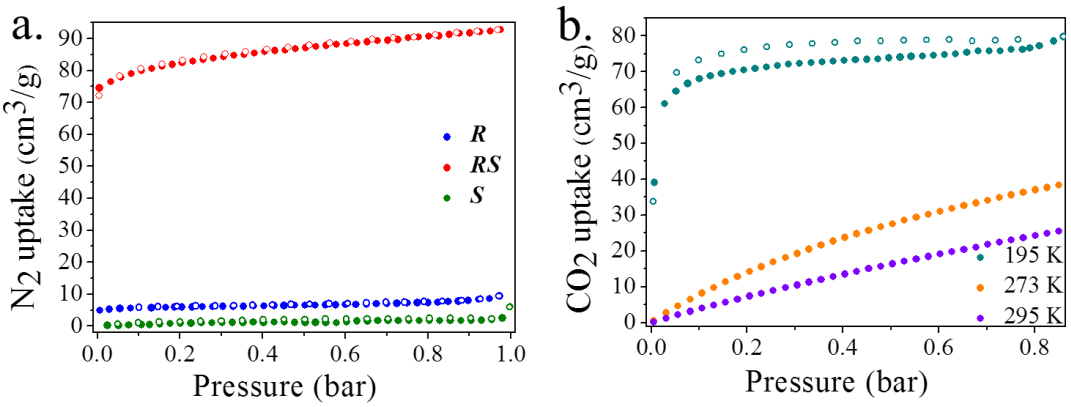

Figure S20: **(**a) N_2 isotherms on ***S***, ***R*** and ***RS*** collected at 77 K up to 1 bar and (b) CO_2 isotherms collected on ***RS*** at 195, 273 and 295 K up to 0.85 bar.

SI 14. Isosteric heat of adsorption

Isosteric heats of adsorption (Q_{st}): The carbon dioxide affinity of ***S*** can be quantitatively reflected by the isosteric heat of adsorption *Qst*, which is calculated utilizing the virial-type expression, using the adsorption branches measured at 273 K and 298 K.[4]

$$\ln P = \ln N + \frac{1}{T}\sum_{i=0}^{m} a_i N^i + \sum_{i=0}^{n} b_i N^i$$

Where :

P: pressure of the adsorption at T_1 = 273 K and T_2 = 298 K

N: amount adsorbed

T: temperature

a_1 and b_1: virial coefficients

m and *n*: represent the number of coefficients required to describe the isotherm.

The values of the virial coefficients a_0 through a_m were then used to calculate the isosteric heat of adsorption using the following expression:

$$Qst = - R\sum_{i=0}^{m} a_i N_i$$

Where :

Qst: Isosteric heat of adsorption

R: gas constant

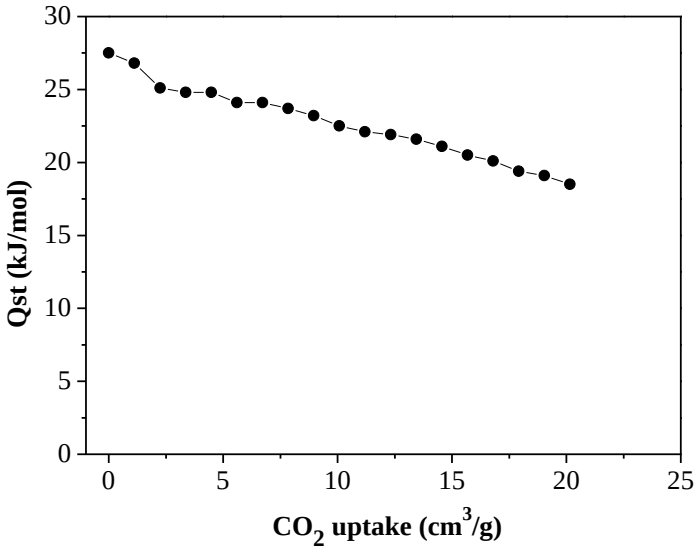

Figure S21: Isosteric heat of adsorption *(Q_{st})* calculated using the virial-type equation and the adsorption branches of the CO_2 isotherms (collected at 273 K and 298 K).

SI 15. Supplementary references

(1) Haridas, V.; Sharma, Y. K.; Naik, S. *European Journal of Organic Chemistry* **2009**, *2009*, 1570.

(2) Guerrero-Martínez, A.; Auguié, B.; Alonso-Gómez, J. L.; Džolić, Z.; Gómez-Graña, S.; Žinić, M.; Cid, M. M.; Liz-Marzán, L. M. *Angewandte Chemie International Edition* **2011**, *50*, 5499.

(3) Berova, N.; Bari, L. D.; Pescitelli, G. *Chemical Society Reviews* **2007**, *36*, 914.

(4) Al-Muhtaseb, S. A.; Ritter, J. A. *Industrial & Engineering Chemistry Research* **1998**, *37*, 684.